https://doi.org/10.5194/nhess-2020-234
Preprint. Discussion started: 9 September 2020

Natural Hazards and Earth System Sciences Discussions

GIS-based topographic reconstruction and geomechanical modelling of the Köfels Rock Slide

Christian Zangerl[1], Annemarie Schneeberger[1,2], Georg Steiner[1,3], Martin Mergili[1,4]

[1]Institute of Applied Geology, University of Natural Resources and Life Sciences (BOKU), Vienna, 1190 Austria
[2]Institute of Geography, University of Innsbruck, Innsbruck, 6020, Austria
[3]Amt der Kärntner Landesregierung, Klagenfurt, 9021, Austria
[4]Department of Geography and Regional Science, University of Graz, Graz, 8010, Austria

Correspondence to: Christian Zangerl (christian.j.zangerl@boku.ac.at)

Abstract.

The Köfels Rock Slide in the Ötztal Valley (Tyrol, Austria) represents the largest known extremely rapid landslide in metamorphic rock masses in the Alps. Although many hypotheses for the trigger were discussed in the past, until now no scientifically proven trigger factor has been identified. This study provides new data about the i) pre-failure and failure topography, ii) failure volume and porosity of the sliding mass, and iii) shear strength properties of the gneissic rock mass obtained by back-calculations. Geographic information system methods were used to reconstruct the slope topographies before, during and after the event. Comparing the resulting digital terrain models leads to volume estimates of the failure and deposition masses of 3.1 km³ and 4.0 km³, respectively and a sliding mass porosity of 26%. For the back-calculations the 2D discrete element method was applied to determine the shear strength properties of the reconstructed basal shear zone. Results indicated that under no groundwater flow conditions, a very low friction angle below24° is required to promote failure, whilst, with groundwater flow, the critical value increase to 28°. Such a low friction angle is unexpected from a rock mechanical perspective for this strong rock and groundwater flow, even if high water pressures are assumed, may not be able to trigger this rock slide. Additional conditioning and triggering factors should be identified by further studies, for example focussing on the impact of dynamic loading.

1 Introduction

In mountain areas, life and property are often put at risk by landslide processes (e.g., Dai et al. 2002; Nadim et al. 2006; Margottini et al. 2013; Sassa et al. 2014). Rapid collapses of huge mountain slopes – and resulting process chains – have repeatedly evolved into catastrophic events (e.g., Evans and DeGraff 2002; Govi et al. 2002; Genevois and Ghirotti 2005; Evans et al. 2009a,b). An adequate understanding of the mechanisms of the initial failure and extremely rapid movement processes is one key for the implementation of effective risk reduction strategies. The analysis of past – even fossil – events may contribute to a better understanding of landslide processes and therefore help to develop and to improve methods for hazard and risk mitigation (Kilburn and Pasuto 2003).

https://doi.org/10.5194/nhess-2020-234
Preprint. Discussion started: 9 September 2020


Natural Hazards and Earth System Sciences Discussions

Known as the largest landslide in metamorphic rock throughout the European Alps, the Köfels Rock Slide represents such a fossil landslide (see Section 2 for a detailed description). In contrast to numerous deep-seated rock slides in foliated metamorphic rocks characterised by movement rates of a few centimetres to decimetres per year and without indications of total slope failure (Zangerl et al. 2015), the Köfels Rock Slide is a prominent case study for a sudden slope failure with extremely rapid movement velocities. This can be clearly demonstrated by the occurrence of frictionites which were found at outcrops on the deposited sliding mass (Erismann et al. 1977). Even though this giant landslide has been subject of numerous studies focussing on the genesis of the frictionites, age of the event, spatial distribution of the source area, volume of the rock slide mass, and geomechanical aspects concerning the trigger and failure mechanisms (e.g., Pichler 1863; Milton 1964; Preuss 1974, 1986; Erismann et al. 1977; Preuss et al. 1987; Erismann and Abele 2001; Brückl et al. 2001, 2010; Brückl and Parotidis 2001, 2005; von Poschinger 2002; Sørensen and Bauer 2003; Prager et al. 2009, Nicolussi et al. 2015), the conditioning and triggering factors of the Köfels Rock Slide remain still unknown and speculative.

Computer models focussing on the rock slide geometry and geomechanical processes may help to increase our understanding of the mechanisms of rock slope failure. Although models are always a rough simplification of reality, some are useful (Box and Draper 1987) to explore specific aspects such as rock slide volumes, slope deformations or critical values of geomechanical parameters at failure. In the context of this study two types of models, i.e. topographical and geomechanical models, are relevant. Brückl et al. (2001) were the first ones who reconstructed the 3D pre-failure topography and failure geometry of the Köfels Rock Slide on the basis of seismic measurements and terrain models and they derived parameters such as failure and deposition volumes, porosity, the initial and average sliding angles and the release of potential energy.

In our study we used new high-resolution (1 m raster data) airborne laser scanning (ALS) based digital terrain models, new geological mapping data and pre-existing data from seismic measurements to re-build and re-analyse the pre- and post-failure topographies and geometries of the rock slide. Based on this topographic reconstruction by using geographic information system (GIS) analysis methods a geometrical-kinematical rock slide model were developed. Conclusions can be made about the failed and deposited volumes, and consequently, the change of rock mass porosity induced by the rapid sliding and fracturing and loosening processes.

Concerning geomechanics of the rock slide at initial failure state and movement several attempts were made to investigate the mechanisms and to back-calculate rock mass properties. Erismann et al. (1977) developed a kinematic and thermodynamic model to explain the energy release necessary for the formation of the frictionites that were found at the Köfels site (see Section 2). Brückl and Parotidis (2001) set up a 2D elastic and elasto-plastic continuum model to estimate the geomechanical rock mass properties of the Köfels Rock Slide. In their approach they applied the 2D finite element method to explore the initial phase of the failure process by studying creeping and strength degradation of the rock mass. The model suggests that the Köfels Rock Slide was formed due to progressive strength softening of the rock mass, which initiates at the foot of the slope and propagates uphill. Furthermore, the model calculations determined surprisingly low friction angles of the rock mass, ranging between 20–24° to induce slope failure. In another approach, Brückl and Parotidis (2005) proposed a model with focus on time-dependent strength degradation and slope failure under low stress regimes such as rock mass creep and subcritical crack

https://doi.org/10.5194/nhess-2020-234
Preprint. Discussion started: 9 September 2020


Natural Hazards and Earth System Sciences Discussions

growth. They suggest that subcritical crack growth is a primary geomechanical process which, after glacier retreat, is able to explain the considerable rock mass strength weakening needed for failure.

However, the extraordinary low strength properties of the rock mass that were back-calculated by 2D continuum approaches for the failure state raise questions:

- How can the strength of such a strong granitic rock mass reduce to such small values needed to promote failure?
- Why do we observe only one such giant and extremely rapid rock slide characterised by a flat to moderately dipping failure surface in Ötztal-Stubai crystalline basement?
- Are there any structural particularities in the Köfels Rock Slide area that may have contributed to slope failure?

Given that, so far, only 2D continuum models have been applied to reconstruct the failure mechanisms of the Köfels Rock Slide we believe that, though representing a valid approach, additional types of models, e.g. discontinuum models, are useful to adequately capture the complexity of the phenomenon. Discontinuum models such as the distinct element method have the advantage that the geometry of the rock slide mass and the discrete basal shear zone can be implemented directly based on geometrical and structural field observations and GIS-reconstructions. Geomechanically, the basal shear zone i.e. stepped rupture surface can be considered in the model as a discrete narrow zone. In order to fill this gap, we set up a 2D discontinuum model of the Köfels Rock Slide, based on the geometry obtained by the topographic model, and by applying the discrete element code UDEC by Itasca (Itasca Consulting Group 2014b). Back-calculations of the critical angle of friction along the basal shear zone assuming no groundwater flow conditions and groundwater flow are conducted under quasi-static conditions. These back-calculations were done to determine the shear strength properties, i.e. friction angle and cohesion, of the predefined and field-based basal shear zone needed to promote failure. The models were performed to explore the influence of fracture water pressure in the rock mass and basal shear zone resulting from exceptional high groundwater levels for provoking this giant landslide.

In addition to the back-calculation of shear strength properties at failure, a geological field survey was performed to search for instability-relevant discontinuities of different origin and scale. This was done to investigate the impact of discontinuities which ideally are dipping moderately towards east, acting as weakness zones and thus reducing the overall rock mass strength. Particular focus was given on the identification of low-strength brittle fault zones composed of gouges and breccia characterised by a high persistence.

Next, we introduce to the study area, the Köfels Rock Slide (Section 2). Then, we explain the methods applied for the topographic reconstruction and geomechanical modelling (Section 3). We present (Section 4) and discuss (Section 5) the results before concluding with the key messages of this study (Section 6).

https://doi.org/10.5194/nhess-2020-234
Preprint. Discussion started: 9 September 2020


Natural Hazards and Earth System Sciences Discussions

2 Study area and data

2.1 Geographic and geologic setting

The Köfels Rock Slide (Figs. 1 and 2) occurred in the central part of the north-south striking Ötztal Valley (Tyrol, Austria), at present at an elevation between 950 m and 1100 m asl. Surrounded by up to 3.000 m high summits, this area is deeply incised in the polymetamorphic Ötztal complex, a major thrust unit belonging to the Upper Austroalpine basement nappes (Prager et al. 2009). Lithologically, different types of metamorphic rocks i.e. paragneisses, quarzites and micaschists with intercalations of orthogneisses, amphibolites and eclogites are encountered (Hammer, 1929; Purtscheller, 1978). The complex ductile and brittle structural setting results from polyphase and heteroaxially deformations and is attributed to at least three distinct orogeneses and their corresponding regional metamorphic overprint. In contrast to numerous petrological and geochronological studies, the brittle deformation history and their related structures of the Ötztal basement was not studied so far in detail, but would be highly relevant for geomechanical purposes. However, Prager et al. (2009) provide some data concerning the discontinuity network in the surroundings of the Köfels Rock Slide.

During the Quaternary period, the Ötztal valley was influenced by repeated glacier fluctuations, causing valley incision, glacial and fluvial erosion as well as sediment accumulation. Valley deepening and steepening leads to substantial stress redistributions in the rock slopes, which in turn initiates time-dependent progressive failure processes in the fractured rock mass and may expose preferentially orientated failure surfaces.

2.2 The Köfels Rock Slide

The age of the Köfels Rock Slide was determined several times through radiocarbon dating of wood buried by the rock slide deposits (Ivy-Ochs et al. 1998), surface exposure dating of rock slide boulders (Kubik et al. 1998) and actually by tree-ring analysis and radiocarbon dating of new wood samples (Nicolussi et al. 2015). The last dating campaign, yielding 9527–9498 cal BP, led to a significant refining of the timing of the Köfels landslide event and even was able to constrain the season during which the event occurred.

The main source of the slide is located in competent fractured orthogneisses (Augengneiss) around the small village Köfels. Only at the southern head scarp area the failure mass is composed of paragneissic rock. The head scarp located at the western slope of the central Ötztal Valley is very steep with inclinations of up to 40–80°. Comprising a failure volume of more than 3 km^3 the Köfels Rock Slide poses a particular event of very rapid large-scale failure in metamorphic rock mass. Typically, such rapid rock slides characterised by a moderately inclined basal failure surface occur in carbonatic rock masses (Prager et al. 2008). The displacement of the sliding rock mass initiated at the east facing slope south of Wenderkogel (see Fig.1 and 2) and stopped at the opposite slope in the east at the entrance of the tributary valley Horlachtal Valley, where it collided with massive bedrock. The centre of mass displacend around 2.6 km (Sørensen and Bauer 2003), reaching a velocity of approx. 50 m/s (Erismann et al. 1977). The main rock slide deposit blocked the Ötztal Valley and formed a prominent valley spur of fractured and disintegrated orthogneiss. Erismann and Abele (2001) proposed that the mass was split into two parts with the

https://doi.org/10.5194/nhess-2020-234
Preprint. Discussion started: 9 September 2020


Natural Hazards and Earth System Sciences Discussions

lower one arresting due to the collision within the steep valley slope and the upper one which continued its movement, thus creating an additional internal sub-horizontal shear zone. The Tauferberg (see Figs.1 and 2) was formed when the upper mass continued its movement towards the Horlachtal valley for approx. one more kilometre and ran up for approx. 100 m. Though plausible, evidence for a distinct internal shear zone was claimed by Preuss (1986), but proof for the existence of such a feature has not yet been found in the field. It seems even more plausible that the immense internal rock mass deformation during the movement and the adaptation to the terrain surface was based on the formation of numerous internal shear zones. The disintegration of the rock mass during the slide event caused a very heterogeneous highly fractured and partly crushed rock mass, with shear zones composed of gouges and breccias and zones with blocks of more than 10 m diameter (Sørensen and Bauer 2003). Furthermore, zones that are characterised by high fracture frequencies only marginally increased in comparison to those commonly observed in undisturbed fractured rock masses. This distinctive fragmentation of rock led to radon gas emissions and locally radioactive springs, which still affects today's population in Umhausen and causes noticably high cancer rates (Purtscheller et al. 1995).

After the slide event, a temporary lake flooded the basin of Längenfeld, impounded by the valley spur (Ampferer 1939). As a result of the flooding backwater sediments were deposited in the basin of Längenfeld as well as in the blocked tributary Horlachtal Valley at Niederthai. According to drilling data from von Klebelsberg (1951) and Ampferer (1939), the lacustrine sediments reach a maximum thickness of 92 m. Later on, the river Ötztaler Ache cut into the rock slide deposits, forming the Maurach gorge by fluvial erosion (see Figs. 1 and 2; Erismann and Abele 2001).

When the mountain slope collapsed, an amount of about $1.6x10^{16}$ J of energy was released. This value was estimated by Erismann and Abele (2001) with respect to volume, density and vertical displacement of the rock mass. The high amount of released energy led to partial melting of the orthogneissic rock at the progressively exposed sliding surface but also around internal shear zones and the development of a fused rock (i.e. pumice, frictinites, hyalomylonites), the presence of which was interpreted in various ways over the years (e.g., Pichler 1863; Preuss 1974; Erismann et al., 1977; Masch et al., 1985; Weidinger et al. 2014).

Though subject of research for more than one century, the question of the causes and maybe the "single" trigger for the Köfels Rock Slide remains still open. Most probably a combination of various conditioning and interacting triggering factors led to the release of this giant slide.

Given that the collapse of Köfels occurred >5 ka years after valley deglaciation, time-dependent progressive failure processes such as sub-critical crack growth and fracture propagation were caused by over-steepening of the valley flanks which is assumed to have provoked unstable conditions in the slope. This long-term disintegration of rock is seen as a prerequisite for the development of a large-scale rock slide (Prager et al. 2009, Brückl and Parotidis 2005, Abele 1994). Moreover, permafrost degradation is suspected to have influenced the failure of many Holocene deep-seated rock slides (Abele 1994) - a phenomenon that gains new relevance considering the degrading permafrost in today's mountains influenced by modern climatic changes (e.g. Gruber and Haeberli 2007, Huggel et al., 2010). To what extent permafrost degradation is able to trigger a deep-seated rock slides characterised by a shear zone at a depth of several hundred metres, is unclear and still under discussion (Nicolussi

https://doi.org/10.5194/nhess-2020-234
Preprint. Discussion started: 9 September 2020


Natural Hazards and Earth System Sciences Discussions

et al. 2015). Abele (1994) and Weidinger (2006) describe active tectonics i.e. earthquakes as one main background condition provoking large rock slide events due to dynamic loading. Considering the present low seismic activity in the Ötztal Valley, Sørensen and Bauer (2003) question an earthquake as a possible trigger for the event.

2.3 Data

An up-to-date digital elevation model (DEM), gained by airborne laser scanning (LiDAR), of the investigated area was obtained from the governmental service for maps of Tyrol, TIRIS, at a spatial resolution of 1 m. Topographic and geologic information on the situation before and after the Köfels Rock Slide are given through studies of von Klebelsberg (1951), Brückl (2001), Heuberger (1994) and Prager et al. (2009). Data from several boreholes from von Klebelsberg (1951) were used in this work. Additionally, reflection and refraction seismic measurements were conducted between 1986 and 1990 (Brückl 1988; Brückl and Heuberger 1993; Brückl et al. 1998; Brückl et al. 2001). In the framework of a hydroelectric power project an investigation drift was drilled into the Tauferberg in 1952 and provides additional information about the geological setting of the site (Brückl et al. 2001; Ascher 1952). Figure 3 provides an overview of the geophysical and drilling data used for the study.

3 Methods

3.1 Reconstruction of rock slide topography, volume and porosity

Three topographic profiles were constructed, based on the drilling and seismic data provided by von Klebelsberg (1951), Heuberger (1994) and Brückl et al. (2001): Profile 1 is set north of the rock slide zone through the basin of Umhausen, Profile 2 lies within the sliding surface, and profile 3 south of the rock slide zone in the basin of Längenfeld (see Figs. 2 and 3).

Fig. 2 and 3 shows the Profiles 1 and 3. The two profiles display the pre-failure topography reconstructed from the seismic and borehole data and the up-to-date situation. The seismic profiles were projected to the topographic sections and transformed into point data used as input for the GIS-based topographic reconstruction. All spatial analysis tasks were performed using the ArcGIS software by ESRI.

For the reconstruction of the past topographic scenarios, an intermediate horizon of the reflection seismic data was assumed as the top of compacted sediments made up of an old valley infill, which was interpreted to be older than the Köfels Rock Slide. These sediments were buried by the rock slide mass and their upper boundary used for the reconstruction of the topographic scenario in the valley as it was before the Köfels Rock Slide. The deepest horizon with a maximum depth of 400 m was interpreted as the compact rock surface – identical with the sliding plane of the rock slide at the flanks of the valley (Brückl et al. 2001).

The available data are then used to three-dimensionally reconstruct four topographic situations, assuming a U-shaped pre-failure valley topography as well as a curved failure surface:

https://doi.org/10.5194/nhess-2020-234
Preprint. Discussion started: 9 September 2020


Natural Hazards and Earth System Sciences Discussions

1. the pre-failure topography before the Köfels Rock Slide event and before the alluvium north and south of the site was deposited;
2. the topography of the failure surface with the deposits completely removed from the model to illustrate the basal shear zone and without the alluvial deposits north and south of the rock slide;
3. the post-failure topography without the alluvial deposits and with the Köfels Rock Slide deposit in the valley before the incision by the Ötztaler Ache;
4. the up-to-date topography where the Maurach gorge has been created by the incision of the Ötztaler Ache into the deposits and the alluvium has been deposited in the basins of Längenfeld and Umhausen (see Fig. 2).

Within the rock slide mass only information from seismic lines and the investigation adit was given. In the failure area only few data were available. The reconstruction of the pre-failure topography of the Köfels Rock Slide was built on the contour lines of the escarpment of the up-to-date DEM. The hypothetic pre-failure slope between the edges of the escarpment was assumed plane. This simple way of reconstruction does not require additional assumptions not supported by observations.

The failure and the deposition volumes of the Köfels Rock Slide mass were computed from the three reconstructed DEMs:

$$V_F = \sum_{i=1}^{i=m} A\left(zi,_1 - z_{i,2}\right), \quad (1)$$

$$V_D = \sum_{i=1}^{i=m} A\left(z_{i,3} - z_{i,2}\right), \quad (2)$$

where V_F and V_D are the failure and deposition volumes, and $z_{i,1}$, $z_{i,2}$ and $z_{i,3}$ represent the reconstructed elevation of the pixel *i*, the numbers referring to the stages given above. *A* is the area of one pixel, *m* is the number of pixels.

Based on the results of the volumetric calculation in ArcGIS, the porosity of the rock mass before and after failure of the Köfels Rock Slide was estimated. Porosity is defined as the ratio of void space to the total volume of soil or rock (Fetter 2001):

$$n = \frac{V_p}{V_s + V_p}, \quad (3)$$

where *n* is the porosity, V_p is the volume of void space and V_s is the volume of solids.

3.2 Discontinuity mapping and rock mass characterisation

In order to characterise the discontinuity network and the rock mass strength a field survey based on outcrop- and scanline mapping was performed at the slopes of the head scarp. Particular focus was given to detect brittle fault zones composed of gouge and breccia, which are dipping moderately towards east and therefore could have acted, at least partly, as the basal shear zone of the Köfels Rock Slide. Estimation of rock mass strength and shear strength of discontinuities was done to provide data for the comparison with results obtained by the numerical modelling study.

https://doi.org/10.5194/nhess-2020-234
Preprint. Discussion started: 9 September 2020


Natural Hazards and Earth System Sciences Discussions

3.3 Back-calculation based on a discontinuum model (2D)

3.3.1 Modelling strategy

A discontinuum model (i.e. discrete element) has not yet been applied for geomechanical modelling of the Köfels Rock Slide (see Section 1). The advantage of discontinuum modelling compared to a continuum approach, is that a distinct, field-based and in relationship to the model size a thin and discrete basal sliding zone which is able to accumulate large shear displacements, can be modelled. In this study we performed back-calculations of the shear strength properties (i.e. critical angle of friction φ_{bs} by assuming a cohesion c_{bs}=0 MPa) of the basal shear zone at failure (A) without pore water pressure and (B) with pore water pressure, induced by ground water flow. We expected the results

1. to enable estimations to be made of the bandwidth of φ_{bs} for the field-based failure surface under the framework of the reconstructed pre-failure topography;
2. to allow conclusions on the role of increased pore water pressure as possible trigger mechanism of the event by evaluating φ_{bs} against typical values of φ of the rock materials and structures involved;
3. to serve as a basis for future analyses such as the impact of dynamic loading on slope stability and its potential for the triggering of the Köfels Rock Slide.

For the numerical study a two-dimensional distinct element model based on the code UDEC (Itasca 2014) was designed. This software tool characterizes a discontinuous rock mass by an assembly of discrete blocks with contacts or interfaces in between. A continuum mesh of finite-difference zones defines the deformability of the rock mass. During the calculation procedure the blocks interact mechanically at their surfaces and corners. Block velocities and displacements are determined, with the calculation procedure being repeated until a balanced state of equilibrium or ongoing failure is reached.

3.3.2 Model geometry, boundary and initial conditions

Profile 2 (see Fig. 2 and 3) was taken for the discrete element (UDEC) modelling. The pre-failure topography was implemented to create the surface of the slope, whilst the topography of the sliding surface provides the input for the basal shear zone (Fig. 5). Blocks were considered as linear elastic defined by Hooke's law, considering components of stress to be linear functions of components of strain (Jaeger et al., 2007). The main deformation within the system takes place through the movement along discontinuities, i.e. shear and normal displacement. Sliding and rotation of blocks, and opening and interlocking of interfaces make up the movement of the mass (Itasca 2014).

Spacing of the joint set was assumed 50 m in the rock slide mass and 150 m in the underlying granitic gneiss block (see Fig. 5). The finite difference mesh in the model was assigned by a size of 25 m in the rock slide mass and 50 m in the underlying granitic gneiss block. Rounding of block corners were applied with a radius of 0.5 m. This avoids the problem of contact overlap, possibly resulting from the interaction of blocks occurring close to or at two opposing block corners (Itasca 2014).

In the modelling scenario (B) a groundwater table was assumed with respect to characteristic groundwater flow patterns where the unsaturated zone between the surface and the water table is typically deep at the head of the slope, whereas the water table at the basis of the slope is close to or at the surface (see Fig. 5; e.g. Fetter 2001).

https://doi.org/10.5194/nhess-2020-234
Preprint. Discussion started: 9 September 2020


Natural Hazards and Earth System Sciences Discussions

No displacement boundaries were applied on the left, right and lower model boundary (Fig. 5). For models with pore water pressure (B), the lower model boundary was set to a no-flow i.e. impermeable boundary. The left and right groundwater model boundary was defined by a hydraulic gradient based on hydrostatic water pressure according to the assumed water table. The maximum water pressure was set to 19.7 MPa at the left boundary along the y-axis and to 8.98 MPa at the right boundary along the y-axis (see Fig. 5). The in-situ stresses were initialised in terms of a vertical gradient based on gravity and the horizontal stresses being half of the vertical stresses by assuming a k-ratio of 0.5. At the model origin (0,0) the two horizontal stresses were assigned to $\sigma_{xx} = \sigma_{zz} = 25.6$ MPa and the vertical stress to $\sigma_{yy} = 51.2$ MPa, respectively.

3.3.3 Material properties

The back-calculations of the friction angle of the basal shear zone were conducted with the assumption of the discontinuities of $\varphi = 30°$ (c=0 MPa) for the granitic gneiss of the failure mass and the underlying block (Table 1). The friction angle of the basal shear zone was varied between 20° and 27° for (A) and between 25° and 32° for (B), by assuming a cohesion of c=0 MPa. A density of $\rho = 2{,}600$ kg/m³ was assigned to all rock materials. Assuming a Young's modulus $E = 40$ GPa and a Poisson's ratio $v = 0.2$ a bulk modulus of 17 GPa and the shear modulus of 22 GPa of the granitic gneiss was obtained. Simplified conditions with a vertical and horizontal fully persistent joint set were implemented to simulate isotropic groundwater flow conditions for (B). Table 1 summarizes the material properties applied to the model.

4 Results

4.1 Reconstruction of rock slide topography, volume and porosity

Figs. 6 and 7 illustrates the results of the three-stage topographic reconstruction of the Köfels Rock Slide. Whilst stage 2 represents a theoretical situation that has never occurred in this way (however, it is necessary to reconstruct the rock slide volumes, see Eqs 1 and 2), the stages 1 and 3 represent hypothetic morphologies directly before and after the event. Note that the very smooth pre-failure topography of the failure area most probably does not resemble the original shape of the mountain slope before failure (see Figs. 6 and 7a) – however, given the fact that there are no data supporting more advanced reconstruction methods, we considerd this approach a reasonable approximation. Stage 4 represents the situation observed today. Comparing Figs. 7c and d indicates those morphologic processes having shaped the site since the event, most significantly the incision of the Maurach gorge by the Ötztaler Ache River into the rock slide deposits and the deposition of lake sediments in the basins of Umhausen and Längenfeld as well as the Horlachtal Valley (see Figs. 1, 2 and 6).

Applying the Eqs. 1 and 2 to the reconstructed topographies, a failure volume of $V_F = 3.1$ km³ and a deposition volume of $V_D = 4.0$ km³ were obtained (Fig. 8). Based on these volumetric reconstructions of failure and deposition masses, considerations about the porosity before and after the Köfels Rock Slide were made. Typical porosities for intact granitic rocks caused by micro-fractures are around 1–2%, not considering any meso-scale joints (Zangerl et al. 2003). Taking into account joints in the rock mass the porosity increase to 2–5% (Fetter 2001). Assuming a pre-failure porosity of the fractured granitic

https://doi.org/10.5194/nhess-2020-234
Preprint. Discussion started: 9 September 2020


Natural Hazards and Earth System Sciences Discussions

rock mass of 5% and a constant volume of the solid content of the rock mass V_s before and after the collapse of the mountain slope, Eq. 3 predicts a porosity of the fractured rock mass after the sliding event of approx. 26%. Consequently, we estimated an increase of the mean porosity from a few % to 26% resulting from the disintegration of the rock mass during the Köfels Rock Slide.

4.2 Discontinuity and rock mass characterisation

The overall structural setting of the Köfels rock slide scarp area has already been comprehensively described in Prager et al. (2019). Nevertheless, in this study new discontinuity data were obtained during an outcrop mapping campaign in the orthogneissic rocks around the central part of the head scarp. Data comprising discontinuity orientation, frequency, spacing, length, roughness and strength were sampled by scanline and outcrop surveys to determine the structural anisotropy and to estimate roughly the strength properties of the rock mass. The orthogneissic rock is foliated, therefore highly anisotropic with a mean dip direction and dip angle of 114/07 (Fig. 1c). At meso-scale, the rock mass is fractured by four joint sets. One primary joint set, labelled as set #1 is dipping moderately towards east varying around a mean dip direction/dip angle of 090/32 (Fig. 1c). Joints assigned to set #1 are dipping sub-parallel to the exposed scarp surface and thus are part of the basal shear zone/surface. Remarkably, these joints feature a medium to very high persistence reaching lengths of several tens of metres and a surface roughness defined as rough and stepped (ISRM 1978). According to the approach of Barton and Choubey (1977) a mean joint roughness coefficient of JRC=10 was determined. Occasionally, some surfaces of fractures orientated sub-parallel to set #1 are coated with Quartz minerals, representing vein fillings which were most likely sheared and exposed during the rock slide events. The appearance of striations on these fractures suggest a tectonic origin, i.e. shear fractures/fault planes. A further dominant joint set (#2) is dipping steeply towards WSW (dip direction/dip angle of 242/70, Fig. 1c). However, in some areas surrounding the head scarp set #2 dips steeply towards east (Fig. 1c). The stepped topography of the scarp flank observed in the upper scarp area originated by intersection of these two joint sets, forming a stepped failure surface. In addition, two less prominent joint sets i.e. set #3 clustering around a mean of 133/47 and overlapping with set #1 as well as set #4 with a mean of 030/65 were measured (Fig. 1c).

Based on field measurements in the orthogneissic rock mass a mean total joint spacing of around 0.6 m and a mean block size of approximately V_b=0.3 m^3 were obtained. Special attention was given during the field campaigns to detect brittle fault zones of tectonic origin with a preferable orientation, dipping moderately to east and with fault zone infillings of gouge and breccia. These brittle fault zones, if available, could have acted as low-strength weakness zones and therefore been responsible to a certain degree for the rock slide formation. Although a detailed exploration of the terrain was carried out, no such structures could be found. In addition, the spatial analysis of high-resolution LiDAR-based digital elevation models (DEM, 1 m raster) provide also no evidence for such brittle faults. On the contrary, most brittle fault zones mapped are inclined steeply and are striking WNW-ESE (major set), ENE-WSW (minor) and NNW-SSE. As already mentioned above, only meso-scale fractures coated with striations were found in the scarp area, representing structures with shear markers. Based on the current level of

https://doi.org/10.5194/nhess-2020-234
Preprint. Discussion started: 9 September 2020


Natural Hazards and Earth System Sciences Discussions

knowledge there is no evidence that low-strength brittle fault zones were involved as part of the basal rupture surface in the initial progressive failure process of the rock slide.

In order to assess the strength of the rock mass, the GSI characterisation method proposed by Cai et al. (2004) and Hoek and Brown (1997) was applied. From field survey a GSI≥55 and from block size/joint spacing a GSI=55 were obtained for the orthogneissic rock. Uniaxial compressive tests performed on orthogneisses show a mean UCS value of 125 MPa (9 tests were performed on similar rocks in the context of a dam project). In order to consider the influence of long-term loading on the strength of the intact rock (rock creeping, sub-critical crack growth) the uniaxial compressive strength is reduced to 40% of the test results, which yields 50 MPa (Damjanac and Fairhurst, 2010). In order to assess the lower limit of the rock mass strength, the GSI was further reduced to 45 by assuming an intact rock parameter m_i=15 (Hoek and Brown, 1997). Based on these parameters and the Hoek-Brown failure criterion a rock mass shear strength of c_{rm}=2 MPa and φ_{rm}=35° was obtained. The intact rock shear strength of orthogneissic rock was determined by triaxial laboratory testing and obviously is much larger in the range of c_i=16 to 41 MPa and φ_i=31 to 40° (tests were performed on similar rocks in the context of a dam project). The shear strength of the joints could not be measured in-situ, and was therefore estimated based on the Barton's empirical approach (Barton and Choubey, 1977). The shear strength of unfilled joints is influenced by the roughness, the strength of the joint surface and the normal stress acting on the discontinuity. On the basis of geometrical considerations and modelling results, it was assumed that the in-situ normal stresses acting on the basal shear zone were in the range between 4 to 18 MPa. According to the method of Barton and Choubey (1977) a friction angle ranging from 32° to 35°, by neglecting cohesion (c=0 MPa), was roughly estimated.

4.3 Discontinuum modelling results

4.3.1 Modelling results without pore water pressure (scenario A)

Values of φ_{bs} = 20°–27° for the basal shear zone were varied for back-calculations in conditions without pore water pressure whilst all other parameters were kept constant. The determination of the critical angle of friction at failure was based on the obtained maximum shear displacement along the basal shear zone and the unbalanced forces of the model, ideally reaching values close to zero. As a result, the transition zone between stable conditions and failure was not a single value and found at approx. 24–25° (φ_{bs}; Fig. 9). Models with φ_{bs} < 23.5° for the basal shear zone did not balanced to equilibrium, and thus indicating ongoing slope failure. Figure 10a shows the spatial distribution of displacement vectors of a model run reaching stabilisation (φ_{bs} = 25°). The maximum displacement values of about 0.25 m were reached at the top of the slope close to the peak. Lower values, ranging around 0.10 m, were reached in the lower part of the slope. The vectors of displacement increased again to values at around 0.25 m at the toe of the slope, indicating larger displacements there than in the middle of the slope. The values of the shear displacement along the basal shear zone were unequally distributed. The largest shear displacements were found at the top of the slope as well as at the slope toe, where the basal shear zone ends, with maximum values of around 0.24 m (see Fig. 10b). Smallest shear displacements were determined in the lower part reaching values below 0.12 m.

https://doi.org/10.5194/nhess-2020-234
Preprint. Discussion started: 9 September 2020


Natural Hazards and Earth System Sciences Discussions

345 **4.3.2 Modelling results with pore water pressure (scenario B)**

The influence of pore water pressure on the behaviour of the slope was investigated by implementing a groundwater table to the model as defined in Section 3.3.2 (modelling scenario B). Results show that the model cannot be balanced with values of $\varphi_{bs} < 28°$ (see Fig. 9). In this case, the transition between stable conditions and failure was at approx. 28–29°. The transition between stable and unstable conditions were reflected in the sudden increase of the maximum shear displacement as shown in
350 the graph in Fig. 9. Exemplarily, the friction angle of the basal shear zone is set to $\varphi_{bs} = 29°$ to further investigate the situation with pore water pressure. Maximum displacement values of approx. 1.80 m are found near the peak of the reconstructed mountain and decrease continuously with decreasing elevation, reaching a minimum of approx. 0.20 m at the toe of the slope (Fig. 11a). The maximum shear displacement along the basal shear zone reached a value of approx. 0.37 m (see Fig. 11b). Shearing takes place at the basal shear zone as well as at vertical discontinuities in the upper part of the failing rock mass. The
355 most pronounced shear displacement is predicted in the middle and lower part of the basal shear zone. As opposed to model run A, the middle to the upper part was characterised by minor shear displacements. Here, shearing along vertical discontinuities of around 0.15 m was computed near the topographic peak of the model.

5 Discussion

5.1 Reconstruction of rock slide topography, geometry, volume and sliding mass porosity

360 Topographic reconstructions, volumetric and porosity calculations of the failure and deposition mass of the Köfels Rock Slide have been made before by Brückl et al. (2001). They concluded from seismic data to physical properties of the rock mass. Based on an empirical relationship given by Watkins et al. (1972) the p-wave velocities were plotted versus depth to estimate the porosity of the deposition mass. On the basis of this calculation a relation between the thickness of the overburden and the porosity of the deposits was developed. The calculations by Brückl et al. (2001) resulted in a post-failure mean depth
365 independent porosity of 23%. With an estimated failure volume of 3.28 km³ and a deposition volume of 3.88 km³, Brückl et al. (2001) calculated a volume increase of 18% due to disintegration, fracturing and loosening of the rock mass by the sliding process. The volume increase obtained by this study is 29% and therefore remarkably larger than obtained by Brückl et al. (2001). This discrepancy indicates that the computed volume increase is very sensitive to the computed failure and deposition volumes. Concerning the porosity of the deposition mass we calculated a value of 26%, a value similar to the 23% of Brückl
370 et al. (2001).

5.2 Geomechanical modelling

In this study a topographic reconstruction was performed to provide a reasonable pre-failure, post-failure and geometrical model of the Köfels Rock Slide for subsequent numerical modelling. Given that slope inclination and rock slide geometry have a large impact on stability and limit-equilibrium, the detailed reconstruction of the pre-failure and post-failure slopes and the
375 slide geometry done herein made possible comprehensive cross- and plausibility checks. The back-calculation of the shear

https://doi.org/10.5194/nhess-2020-234
Preprint. Discussion started: 9 September 2020


Natural Hazards and Earth System Sciences Discussions

strength of the basal shear zone, assuming a cohesion of zero, in the present study results in values of $\varphi_{bs} \leq 24°$ without pore water pressure and $\varphi_{bs} \leq 28°$ with pore water pressure. Consequently, given that the imposed boundary conditions, rock mass parameters and water pressure are valid, the friction angle of the sliding surface may be constrained to the range φ_{bs} = 24°–28°.

Brückl und Parotidis (2001) gained a value of the rock mass friction angle (φ_{rm}) between 20° and 24° from geomechanical continuum modelling of the Köfels Rock Slide. In a later approach, Brückl and Parotidis (2005) modelled the Köfels Rock Slide by applying a finite 2D-element method and focussing on modelling of the rock slide failure geometry. For their approach, they assumed a friction angle of φ_{bs} = 28°, without considering pore water pressure.

A preliminary comparison with 3D limit-equilibrium slope stability models (r.slope.stability; Mergili et al. 2013, 2014) indicates that the safety factors yielded by these models are equal to 1 at approx. 1–3° higher values of φ, compared to the critical values derived in our discontinuum approach. More research is necessary to explore this issue, and particularly the influence of using 3D models.

The back-calculated friction angles of the basal shear zone required to induce slope failure are ranging from 24° to 28°. In comparison empirical estimations of the rock mass strength based on the GSI approach by Hoek and Brown (1997) show that the obtained shear strength values of the rock mass of c_{rm}=2 MPa and φ_{rm}=35° are far too high to promote slope failure under static conditions.

Concerning unfilled and rough joints in granitic rocks the friction angle guessed by Barton and Choubey (1977) is several degrees higher than needed for slope failure. In-situ shear strength data for rough, unfilled joints in granitic rocks published by Fishmann (2004) show a remarkably high friction angle of φ_j=44° linked to a cohesion of c_j=0.08 and c_j=0.14 MPa, respectively. Grøneng et al. (2009) determined the shear strength of unfilled rock joints focusing on the Åknes rock slide in Norway by applying Barton-Bandis empirical equation. Applying their proposed parameters to an in-situ stress range from 4 to 18 MPa results in a friction angle between 31 and 36°. Grasselli (2001) performed shear tests on fresh tensile rock joints of gneisses and granites, additionally by applying up to 6 shear test cycles on the same samples. He measured values between 39° and 69° for the peak friction angle and values between 35° and 57° for the residual friction angle. Both, Byerlee (1978) and Hencher et al. (2011) determined a (basic) friction angle of around 40° for granitic rock joints.

In addition, field observations confirm that the fractures have a persistence in the scale of meters to tens of meters, and therefore it is assumed that the rock mass at the Köfels Rock Slides is characterised by intact rock bridges. It is widely accepted that intact rock bridges, if present, increase the shear strength of a rock mass (Jennings 1970, Einstein et al. 1983). Intact rock bridge failure is complex and usually not simply related to in-plane shear along the fractures, and is characterised by time-dependent progressive failure processes (sub-critical crack growth, Atkinson 1984, 1987). Nevertheless, conceptually and in the context of the Köfels Rock Slide intact rock bridges would further increase the overall rock mass strength of the slope, also when considering long-term conditions.

So far, the only possible geological discontinuity type which displays shear strength properties low enough to allow for slope failure under static conditions are pre-existing brittle fault zones composed with infillings of gouge and breccia. The parameters

https://doi.org/10.5194/nhess-2020-234
Preprint. Discussion started: 9 September 2020

back-calculated by numerical modelling correspond reasonably well with the bandwidth of published values, ranging from 19° to 30°, observed for shear zones in crystalline rocks (Engl et al. 2008, Strauhal et al. 2017). However, our detailed geological field investigation and structural analyses of the high-resolution digital elevation models could indeed identify such structures in the rock mass, but not such ones which are dipping moderately towards east and are thus favourably aligned to promote the rock slide formation.

For example, an additional geological factors reducing the rock mass strength by rock mass fracturing and weakening of large rock slopes to depths of several hundred metres is related to deep-seated block or flexural toppling processes (Amann 2006, Casson et al. 2003, Zangerl et al. 2015). Deep-seated toppling occurs when steeply inclined structures are present and this failure mechanism is often observed in foliated metamorphic rock mass with low to moderate strengths (paragneisses, schists and phyllites). However less common, but still observed is toppling in granitic gneisses when foliation as well as joint planes and fault zones are closely spaced and steeply dipping into the slope (Amann 2006). Structural mapping by Prager et al. (2010) and this study in the surrounding of the scarp confirm steeply dipping NNW-SSE striking joints and faults. Though structurally possible, it is questionable if deep-seated toppling is a preparatory mechanism for the Köfels rock mass failure, because no clear geomorphological and structural indicators for toppling were found in the surrounding of the scarp.

Based on the results of the numerical modelling study it is inconceivable that slope failure occurred under pure static conditions, even when a high groundwater table, causing extraordinary high pore pressures, is assumed. Apart from that permafrost degradation due to climate warming has often been discussed as a relevant factor for slope failure in rock masses. So far it is widely accepted that permafrost degradation can alter the rock mass strength by ice melting and temperature changes (Dramis et al. 1995, Fischer et al. 2006, Huggel et al. 2012, Krautblatter et al. 2013). According to the time-depended rock-ice mechanical model proposed by Krautblatter et al. 2013 it is assumed that ice-rock mechanical processes are more relevant for rock slope failures at shallow depths (less than 20 m) whereas rock-rock mechanical processes are dominating at greater depth. Considering this geomechanical concept in relationship to the great depth of the rupture surface of several hundred metres, as well as the time lag of two millennia between Holocene warming and slope failure (Nicolussi et al. 2015), permafrost degradation acting as major trigger of the Köfels rock slide is unlikely. Based on the findings of this study, climate-driven triggering factors characterised by periods of increased precipitation rates or permafrost degradation were probably too weak to provoke such a large-scale slope failure.

One interesting observation was done by Nicolussi et al. 2015 who performed precise age-dating of the 3.1 km^3 large Köfels rock slide based on tree-ring analysis and radiocarbon dating, constraining the event to 9527–9498 cal BP. Remarkably, the new age bandwidth is close to the age of the Flims landslide ranging from 9480–9430 cal BP, the largest rock slide in the Alps, comprising a volume of 8–12 km^3 (Poschinger and Kippel 2009). Furthermore, a few more events occurring in the eastern alps show ages clustering within this period (Prager et al. 2008, Borgatti and Soldati 2010). The close temporal relationship of failure between the Köfels and Flims Rock Slide raises the question whether dynamic loading due to earthquake shaking was able to trigger two of the largest rock slides in the Alps, located about 130 km apart. Up to now it could not be proven if a high-magnitude earthquake has been happened at this time (palaeo-seismic records are incomplete). Furthermore, it is not clear

https://doi.org/10.5194/nhess-2020-234
Preprint. Discussion started: 9 September 2020


Natural Hazards and Earth System Sciences Discussions

how strong the earthquake must have been and whether this hypothesis can be in accordance with seismo-tectonic considerations of the Alps. Conceptually, it would be expected that a large earthquake triggering these two extremely large rock slides would have caused numerous (smaller) events, dating with the same age with failure locations somewhere in between. Thus, we suggest further investigations comprising palaeo-seismic analyses, age-dating, geotechnical shear testing of material from ruptures surfaces, and dynamic numerical modelling efforts in order to shed light on these aspects.

6. Conclusions

Based on geologic, geophysical and topographic constraints, we reconstructed three topographic stages of the Köfels Rock Slide: i) the pre-failure topography with the reconstructed mountain peak, ii) the topography demonstrating the sliding surface without rock slide deposit, iii) the post-failure topography with the deposits in the valley but before their incision by the river Ötztaler Ache. For the failure volume a value of 3.1 km³ is gained, the deposition volume is calculated as about 4.0 km³. These values are very close to those derived by Brückl et al. (2001), leading to the conclusion that the estimates gained of the volumes are sufficiently robust.

Knowledge on the volume increase of the rock mass during sliding is less robust, as the derived values react very sensitive even to small variations in the failure and deposition volumes. Whilst Brückl et al. (2001) come to an increase in volume by 18%, our study suggests an increase by 29%. The porosity of the failed rock slide mass increased to a mean of 26%, with wide variations.

The shear strength of the basal shear zone at failure in conditions without and with pore water pressure is back-calculated by the two-dimensional distinct element code UDEC. The back-calculation study is based on the assumption of a continuous basal shear zone derived from field mapping and high resolution digital elevation models and a cohesion of zero, resulting in values of $\varphi_{bs} \leq 24°$ without pore water pressure and $\varphi_{bs} \leq 28°$ with pore water pressure. However, field observations suggest that a continuous basal shear zone may have formed during the initial failure stage of the slide, but there is no evidence for a pre-existing zone of weakness promoting slope failure. Comparisons of back-calculated shear strength of the basal shear zone with values roughly assessed for the fractured granitic rock mass show that slope failure under static conditions is unlikely, even under high pore pressures. Additional triggering factors, for example impact of dynamic loading have to be considered in further investigations.

Acknowledgements

This study was part of the alpS research projects ‘ProMM’ and ‘AdaptInfra’, which were supported by TIWAG, geo.zt, ILF Consulting Engineers and the Austrian Research Promotion Agency (COMET-program). The alpS-K1-Centre was supported

by Federal Ministries BMVIT and BMWFW as well as the States of Tyrol and Vorarlberg in the framework of "COMET-
475 Competence Centers for Excellent Technologies". COMET is processed through FFG.

References

Abele, G.: Large rockslides: their causes and movements on internal sliding planes. Mt Res Dev 14:315–320, DOI: 10.2307/3673727, 1994.

Amann, F.: Großhangbewegung Cuolm da Vi (Graubünden, Schweiz). Geologisch-geotechnische Befunde und numerische
480 Untersuchungen zur Klärung des Phänomens. Dissertation, Friedrich-Alexander Universität Erlangen-Nürnberg, p. 206, 2006.

Ampferer, O.: Über die geologischen Deutungen und Bausondierungen des Maurach Riegels im Ötztal. Geologie und Bauwesen 11:25–43, 1939.

Ascher, H.: Neuer Sachbestand und Erkenntnisse über das Bergsturzgebiet von Köfels. Geologie und Bauwesen 19:128–134, 1952.

485 Atkinson, B.K.: Subcritical crack growth in geological materials. Journal of Geophysical Research 89 (B6): 4077-4114, https://doi.org/10.1029/JB089iB06p04077, 1984.

Atkinson, B.K.: Introduction to fracture mechanics and its geophysical applications. In: Atkinson BK (ed), Fracture mechanics of rock, Academic Press, 1-26, 1987.

Borgatti, L. and Soldati, M.: Landslides as a geomorphological proxy for climate change: a record from the Dolomites
490 (northern Italy). Geomorphology 120, 56–64, https://doi.org/10.1016/j.geomorph.2009.09.015, 2010.

Brückl, E. and Parotidis, M.: Estimation of large-scale mechanical properties of a large landslide on the basis of seismic results. Rock Mech Min Sci 38:877–883, https://doi.org/10.1016/S1365-1609(01)00053-3, 2001.

Brückl, E. and Parotidis, M.: Prediction of slope instabilities due to deep-seated gravitational creep. Nat Hazards Earth Syst Sci 5:155–172, 2005.

495 Brückl, E. and Heuberger, H.: Reflexionsseismische Messungen am Bergsturz von Köfels. Geologie des Oberinntaler Raumes – Schwerpunkt Blatt 144 Landeck:156–158. Geologische Bundesanstalt, Vienna, 1993.

Brückl, E., Brückl, J. and Heuberger, H.: Present structure and prefailure topography of the giant rockslide of Köfels. Zeitschrift für Gletscherkunde und Glazialgeologie 37(1):49–79, https://doi.org/10.3997/2214-4609.201407174, 2001.

Brückl, E., Brückl, J., Chwatal, W. and Ullrich, C.: Deep alpine valleys: examples of geophysical explorations in Austria.
500 Swiss J Geosci 103:329–344, https://doi.org/10.1007/s00015-010-0045-x, 2010.

Byerlee, J.: Friction of rocks. Pure Appl Geophys 116:615–626, https://doi.org/10.1007/978-3-0348-7182-2_4, 1978.

Casson, B., Delacourt, C., Baratoux, D. and Allemand, P.: Seventeen years of the ‘‘La Clapière’’ landslide evolution analysed from ortho-rectified aeri-al photographs. Engineering Geology 68: 123-139, https://doi.org/10.1016/S0013-7952(02)00201-6, 2003.

https://doi.org/10.5194/nhess-2020-234
Preprint. Discussion started: 9 September 2020

505 Dai, F.C., Lee, C.F. and Yip Ngai, Y.: Landslide risk assessment and management: an overview. Engineering Geology 64(1):65–87, https://doi.org/10.1016/S0013-7952(01)00093-X, 2002.

Einstein, H.H., Veneziano, D., Baecher, G.B. and O'Reilly, K.J.: The Effect of Discontinuity Persistence on Rock Slope Stability. International Journal of Rock Mechanics and Mining Sciences, Vol. 20, No. 5, pp. 227-236, https://doi.org/10.1016/0148-9062(83)90003-7, 1983.

510 Engl, D.A., Fellin, W. and Zangerl, C.: Scherfestigkeiten von Scherzonen-Gesteinen – Ein Beitrag zur geotechnischen Bewertung von tektonischen Störungen und Gleitzonen von Massenbewegungen. Bulletin für Angewandte Geologie 13(2):63–81, 2008.

Erismann, T.H. and Abele, G.: Dynamics of Rockslides and Rockfalls. Springer, Berlin, 2001.

Erismann, T.H., Heuberger, H. and Preuss, E.: Der Bimsstein von Köfels (Tirol), ein Bergsturz-"Friktionit". Tschermaks
515 Mineralogische und Petrographische Mitteilungen 24:67–119, https://doi.org/10.1007/BF01081746, 1977.

Evans, S.G., Bishop, N.F., Fidel Smoll, L., Valderrama Murillo, P., Delaney, K.P. and Oliver-Smith, A.: A re-examination of the mechanism and human impact of catastrophic mass flows originating on Ne-vado Huascarán, Cordillera Blanca, Peru in 1962 and 1970. Engineering Geology 108:96–118, https://doi.org/10.1016/j.enggeo.2009.06.020, 2009a.

Evans, S.G., Roberts, N.J., Ischuk, A., Delaney, K.B., Morozova, G.S. and Tutubalina, O.: Landslides triggered by the 1949
520 Khait earthquake, Tajikistan, and associated loss of life. Engineering Geology 109:195–212, https://doi.org/10.1016/j.enggeo.2009.08.007, 2009b.

Evans, S.G. and DeGraff, J.V.: Catastrophic landslides: Effects, occurrence, and mechanism. Geol Soc Am Rev Eng Geol 15, 2002.

Fetter, C.W.: Applied Hydrogeology. Vol. 4. Prentice Hall Inc., New Jersey, 2001.

525 Fischer, L., Kääb, A., Huggel, C., Noetzli, J.: Geology, glacier retreat and permafrost degradation as controlling factors of slope instabilities in a high-mountain rock wall: the Monte Rosa east face Nat. Hazards Earth Syst. Sci., 6, 761–772, https://doi.org/10.5194/nhess-6-761-2006, 2006.

Genevois, R. and Ghirotti, M.: The 1963 Vaiont Landslide. Giornale di Geologia Applicata 1:41–52, doi: 10.1474/GGA.2005-01.0-05.0005, 2005.

530 Govi. M, Gullà, G. and Nicoletti, P.G.: Val Pola rock avalanche of July 28, 1987, in Valtellina (Central Italian Alps). In: Evans SG, DeGraff JV (eds) Catastrophic landslides: Effects, occurrence, and mechanism. Geol Soc Am Rev Eng Geol 15:71–89, 2002.

Hencher, S.R., Lee, S.G., Carter, T.G. and Richards, L.R.: Sheeting Joints: Characterisation, Shear Strength and Engineering. Rock Mech Rock Eng (2011) 44:1–22, https://doi.org/10.1007/s00603-010-0100-y, 2011.

535 Heuberger, H. The giant landslide of Köfels, Ötztal, Tyrol. Mount Res Dev 13(4):290–294, 1994.

Huggel, C., Clague, J.J. and Korup, O.: Is climate change responsible for changing landslide activity in high mountains? Earth Surf. Process. Landforms 37, 77–91, https://doi.org/10.1002/esp.2223, 2012.

Itasca: UDEC - Universal distinct element code, Version 6.0. Minneapolis, ItascaConsultingGroup, 2014.

Ivy-Ochs, S., Heuberger, H., Kubik, P.W., Kerschner, H., Bonani, G., Frank, M., Schlüchter, C.: The age of the Köfels event. Relative, 14C and cosmogenic isotope dating of an early holocene landslide in the central alps (Tyrol, Austria). Zeitschrift für Gletscherkunde und Glazialgeologie 34:57–68, 1998.

Jaeger, J.C., Cook, N.G.W. and Zimmermann, R.W.: Fundamentals of Rock Mechanics. Vol. 4. Blackwell Publishing, Malden, Mass, 2007.

Jennings, J.E.: A Mathematical Theory forthe Calculation ofthe Stability of Open Case Mines. Proc. Symp. on the Theoretical Background to the Planning of Open Pit Mines. pp. 87-102, Johannesburg, 1970.

Kilburn, C.R.J. and Pasuto, A.: Major risks from rapid, large-volume landslides in Europe (EU Project RUNOUT). Geomorphology 54:3–9, https://doi.org/10.1016/S0169-555X(03)00050-3, 2003.

Krautblatter, M., Funk, D., and Günzel, F.K.: Why permafrost rocks become unstable: A rock-ice-mechanical model in time and space. Earth Surf. Process. Landforms 38:876–887, https://doi.org/10.1002/esp.3374, 2013.

Kubik, P.W., Ivy-Ochs, S., Masari, J., Frank, M. and Schlüchter, C.: 10Be and 26Al production rates deduced from an instantaneous event within the dendro-calibration curve, the landslide of Köfels, Ötz Valley, Austria. Earth Planet Sci Lett 161:231–241, https://doi.org/10.1016/S0012-821X(98)00153-8, 1998.

Kveldsvik, V., Kaynia, A.M., Nadim, F., Bhasin, R., Nilsen, B. and Einstein H.H.: Dynamic distinct-element analysis of the 800 m high Aknes rock slope. Int J Rock Mech Min Sci 46(4):686–698, https://doi.org/10.1016/j.ijrmms.2008.10.007, 2009.

Margottini, C., Canuti, P. and Sassa, K.: Landslide Science and Practice. 7 volumes. Springer, Berlin, Heidelberg, 2013.

Mergili, M., Marchesini, I., Rossi, M., Guzzetti, F. and Fellin, W.: Spatially distributed three-dimensional slope stability modelling in a raster GIS. Geomorphology 206:178–195, https://doi.org/10.1016/j.geomorph.2013.10.008, 2014.

Mergili, M., Marchesini, I., Alvioli, M., Metz, M., Schneider-Muntau, B., Rossi, M. and Guzzetti, F.: A strategy for GIS-based 3-D slope stability modelling over large areas. Geosci Model Dev Disc 7:5407–5445, doi:10.5194/gmd-7-2969-2014, 2014.

Milton, D.J.: Fused rock from Köfels, Tyrol. Tschermaks mineralogische und petrographische Mitteilungen 9:86–94, https://doi.org/10.1007/BF01127777, 1964.

Nadim, F., Kjekstad, O., Peduzzi, P., Herold, C. and Jaedicke C.: Global landslide and avalanche hotspots. Landslides 3(2):159–173, https://doi.org/10.1007/s10346-006-0036-1, 2006.

Nicolussi, K., Spötl, C., Thurner, A., Reimer, P.J.: Precise radiocarbon dating of the giant Köfels landslide (Eastern Alps, Austria), Geomorphology, Volume 243, Pages 87-91, https://doi.org/10.1016/j.geomorph.2015.05.001, 2015.

Pichler, A.: Zur Geognosie Tirols II. Die vulkanischen Reste von Köfels. Jahrbuch der Geologischen Reichsanstalt in Wien 13:591–594, 1863.

Pirkl, H.R.: Die westlichen Zentralalpen (von der Silvretta zum Brenner). In: Oberhauser R, and geologische Bundesanstalt (eds) Der geologische Aufbau Österreichs:332–347. Springer, Vienna, New York, 1980.

Poschinger, A. and Kippel, T.: Alluvial deposits liquefied by the Flims rock slide. Geomorphology 103 (2009) 50–56, https://doi.org/10.1016/j.geomorph.2007.09.016, 2009.

https://doi.org/10.5194/nhess-2020-234
Preprint. Discussion started: 9 September 2020


Natural Hazards and Earth System Sciences Discussions

Prager, C., Zangerl, C., Patzelt, G. and Brandner, R.: Age distribution of fossil landslides in the Tyrol (Austria) and its surrounding areas. Nat. Hazards Earth Syst. Sci. 8, 377–407, https://doi.org/10.5194/nhess-8-377-2008, 2008.

Prager, C., Zangerl, C. and Nagler, T.: Geological controls on slope deformations in the Köfels rockslide area (Tyrol, Austria). Austrian J Earth Sci 102(2):4–19, 2009.

Preuss, E., Masch, L. and Erismann, T.H.: Friktionite - Natürliches Glas aus der Reibungsschmelze sehr großer Bergstürze (Köfels, Tirol - Langtang, Nepal). Proceedings of the 2nd International Conference on Natural Glasses, Prague:1–4. Charles University, Prague, 1987.

Preuss, E.: Der Bimsstein von Köfels im Ötztal/Tirol – Die Reibungsschmelze eines Bergsturzes. Vol. 39. Verein zum Schutze der Alpenpflanzen und -Tiere, Munich, 1974.

Preuss, E.: Gleitflächen und neue Friktionitfunde im Bergsturz von Köfels im Ötztal, Tirol. Material und Technik – Schweizerische Zeitschrift für Werkstoffe, Betriebsstoffe, Materialprüfung und Messtechnik 3. Schweizerischer Verband für die Materialprüfung der Technik (SVMT), 1986.

Purtscheller. F., Pirchl, T., Sieder, G., Stingl, V., Tessadri, T., Brunner, P., Ennemoser, O. and Schneider, P.: Radon emanations from giant landslides of Koefels (Tyrol, Austria) and Langtang Himal (Nepal). Environ Geol 26: 32–38, https://doi.org/10.1007/BF00776029, 1995.

Sassa, K., Canuti, P., and Yin, Y.: Landslide Science for a Safer Geoenvironment. 3 volumes. Springer, Cham, Heidelberg, New York, Dordrecht, London, 2014.

Sørensen, S.A. and Bauer B.: On the dynamics of the Köfels sturzstrom. Geomorpholgy 54:11– 19, https://doi.org/10.1016/S0169-555X(03)00051-5, 2003.

Stutzer, O.: Die Talweitung von Köfels im Ötztal (Tirol) als Meteorkrater. Zeitschrift der Deutschen Geologischen Gesellschaft 88:523–525, 1936.

Suess, F.E.: Der Meteor-Krater von Köfels beim Umhausen im Ötztale, Tirol. Neues Jahrbuch für Mineralogie, Geologie und Paläontologie, Abh., 72:98–155, 1937.

von Klebelsberg, R.: Das Becken von Längenfeld im Ötztal. Ein Beispiel für Geologie und Kraftwerksplanung. Schlern-Schriften 77:399–422, 1951.

von Klebelsberg, R.: Geologie von Tirol. Gebrüder Borntraeger, Berlin, 1935.

von Poschinger, A.: Large rockslides in the Alps: A commentary on the contribution of G. Abele (1937-1994) and a review of some recent developments. In: Evans SG, DeGraff JV (eds), Catastrophic Landslides: Effects, Occurence, and Mechanisms. Geol Soc Am Rev Eng Geol 15:237–257, 2002.

Weidinger, J.T.: Predesign, failure and displacement mechanisms of large rockslides in the Annapurna Himalayas, Nepal. Engineering Geology 83: 201–216, https://doi.org/10.1016/j.enggeo.2005.06.032, 2006.

Weidinger, J.T., Korup, O., Munack, H., Altenberger, U., Dunning, S.A., Tippelt, G. and Lottermoser, W.: Giant rockslides from the inside. Earth Planet Sci Lett 389:62–73, https://doi.org/10.1016/j.epsl.2013.12.017, 2014.

https://doi.org/10.5194/nhess-2020-234
Preprint. Discussion started: 9 September 2020


Natural Hazards and Earth System Sciences
Discussions

Zangerl C, Eberhardt E, Evans KF, Loew S (2003) Analysis of Subsurface Subsidence in Crystalline Rock above the Gotthard Highway Tunnel, Switzerland. Swiss Federal Institute of Technology (ETH), Zurich.

Zangerl, C., Chwatal, W. and Kirschner, H.: Formation processes, geomechanical characterisation and buttressing effects at the toe of deep-seated rock slides in foliated metamorphic rock. Geomorphology. 243: 51-64, https://doi.org/10.1016/j.geomorph.2015.03.030, 2015.

https://doi.org/10.5194/nhess-2020-234
Preprint. Discussion started: 9 September 2020

Natural Hazards and Earth System Sciences
Discussions
Open Access
EGU

Figures

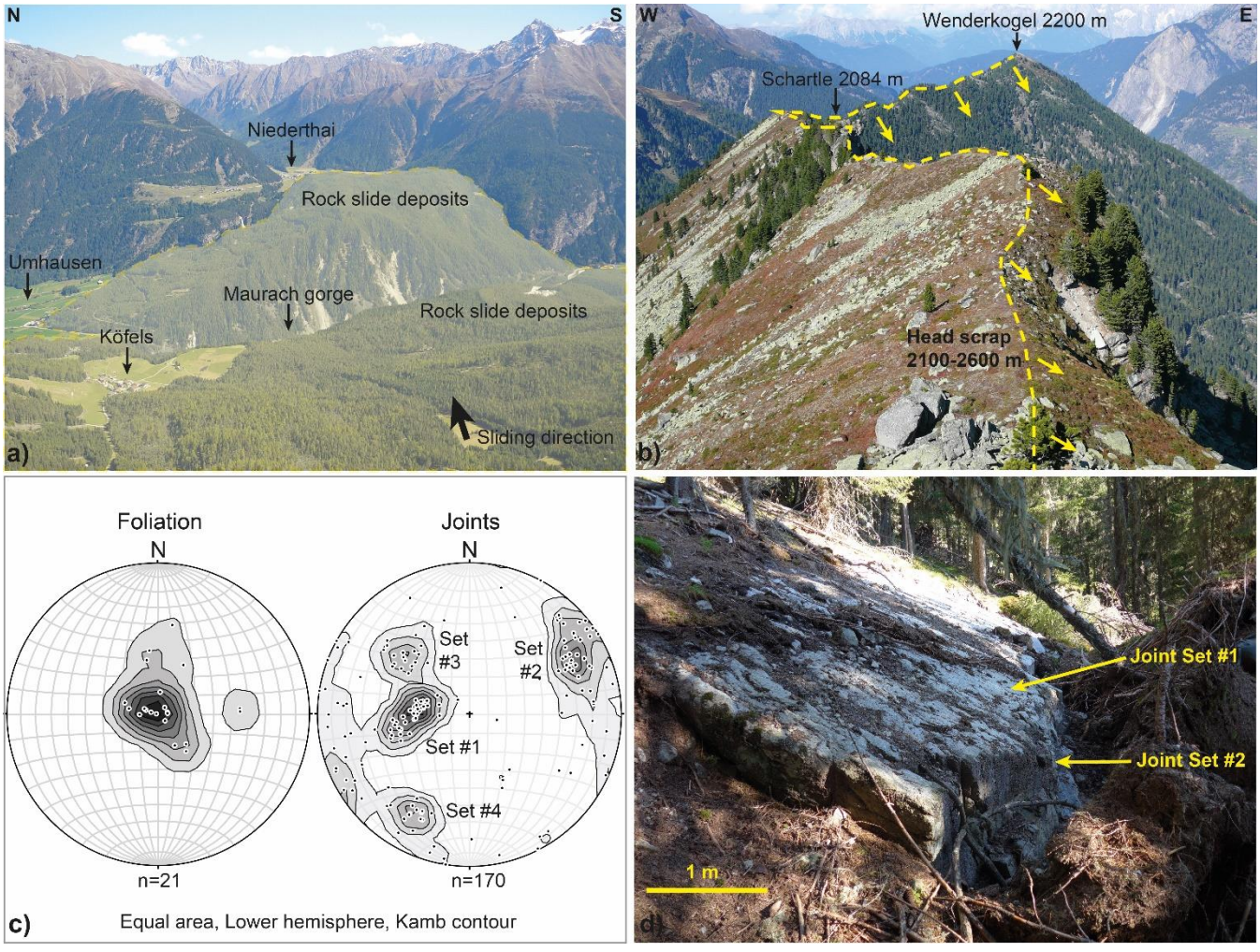

615 Figure 1. a) Panoramic view of the Köfels Rock Slide deposits from head scarp towards E with the Maurach Gorge cutting through the deposits (centre) and the backwater sediments in Niederthai (right), b) View of the head scarp from S to N, c) Measured foliation and joint planes (poles to planes) in the surroundings of the central part of the head scarp, and d) outcropping rupture surface formed along a moderately dipping plane of joint set #1 and linked with joint set #2 (stepped failure plane).

620

https://doi.org/10.5194/nhess-2020-234
Preprint. Discussion started: 9 September 2020

Natural Hazards and Earth System Sciences
Discussions
Open Access
EGU

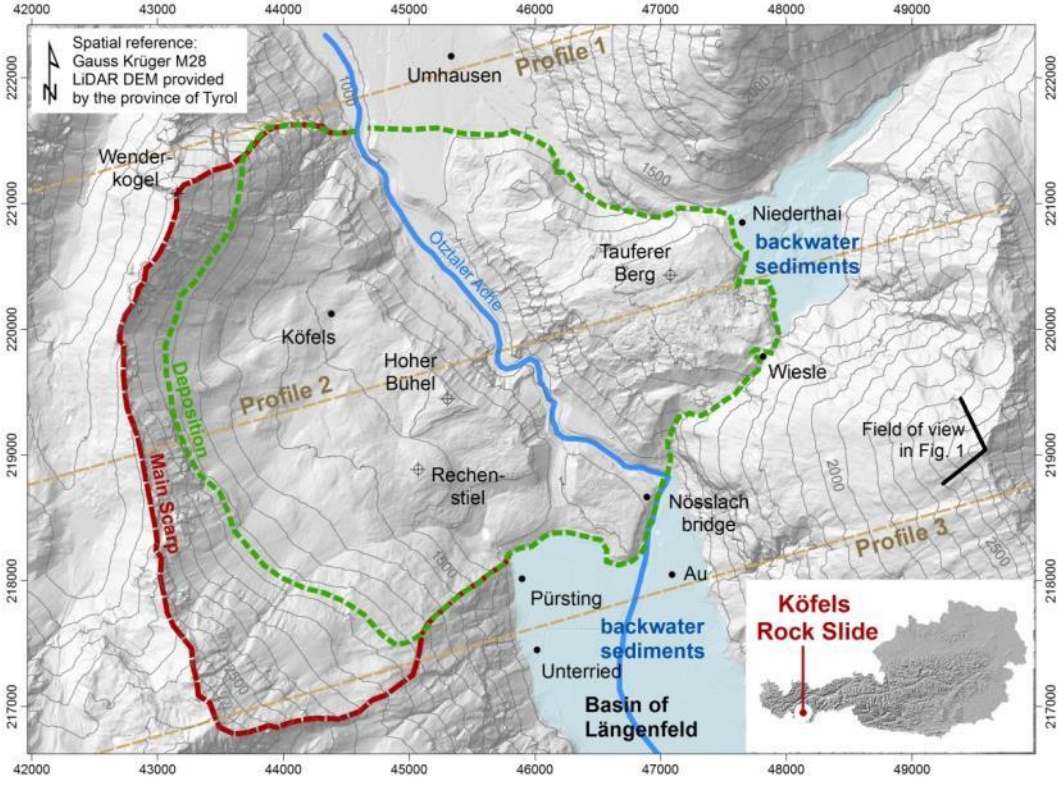

Figure 2: Overview map of the Köfels Rock Slide area.

https://doi.org/10.5194/nhess-2020-234
Preprint. Discussion started: 9 September 2020

Natural Hazards and Earth System Sciences
Discussions
Open Access
EGU

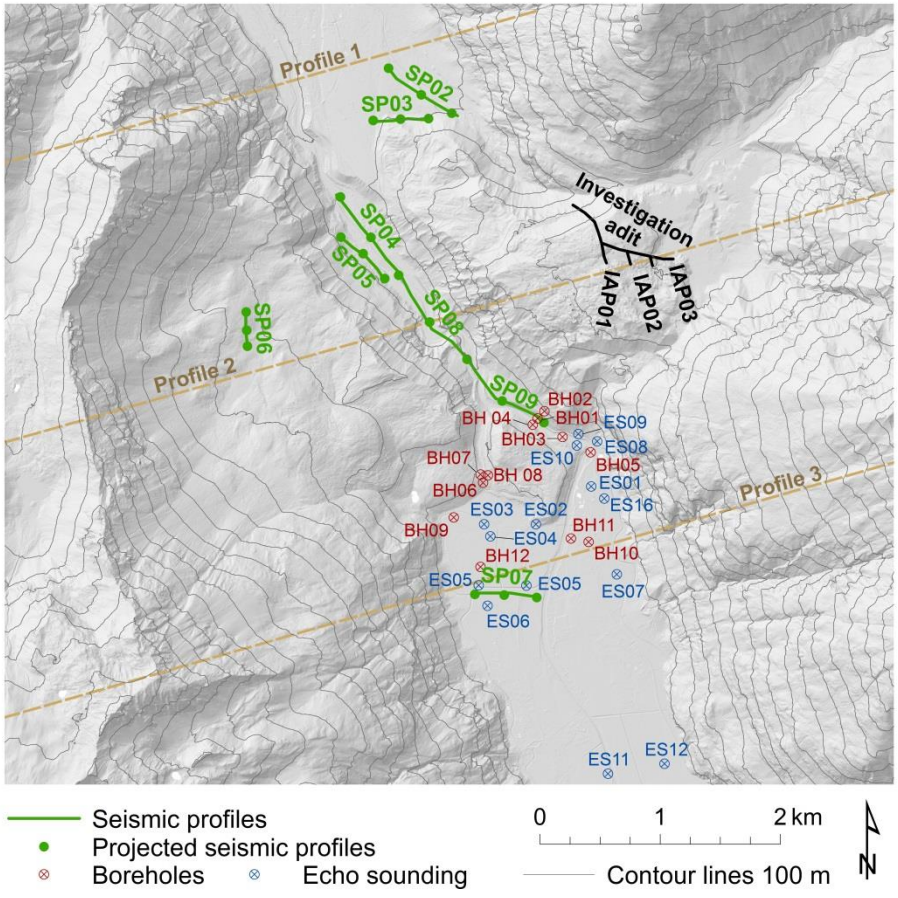

625 Figure 3: Borehole data (BH), echo-sounding (ES) and seismic profiles (SP) used for the topographic reconstruction of the Köfels Rock Slide.

https://doi.org/10.5194/nhess-2020-234
Preprint. Discussion started: 9 September 2020

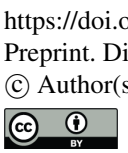

Natural Hazards and Earth System Sciences
Discussions

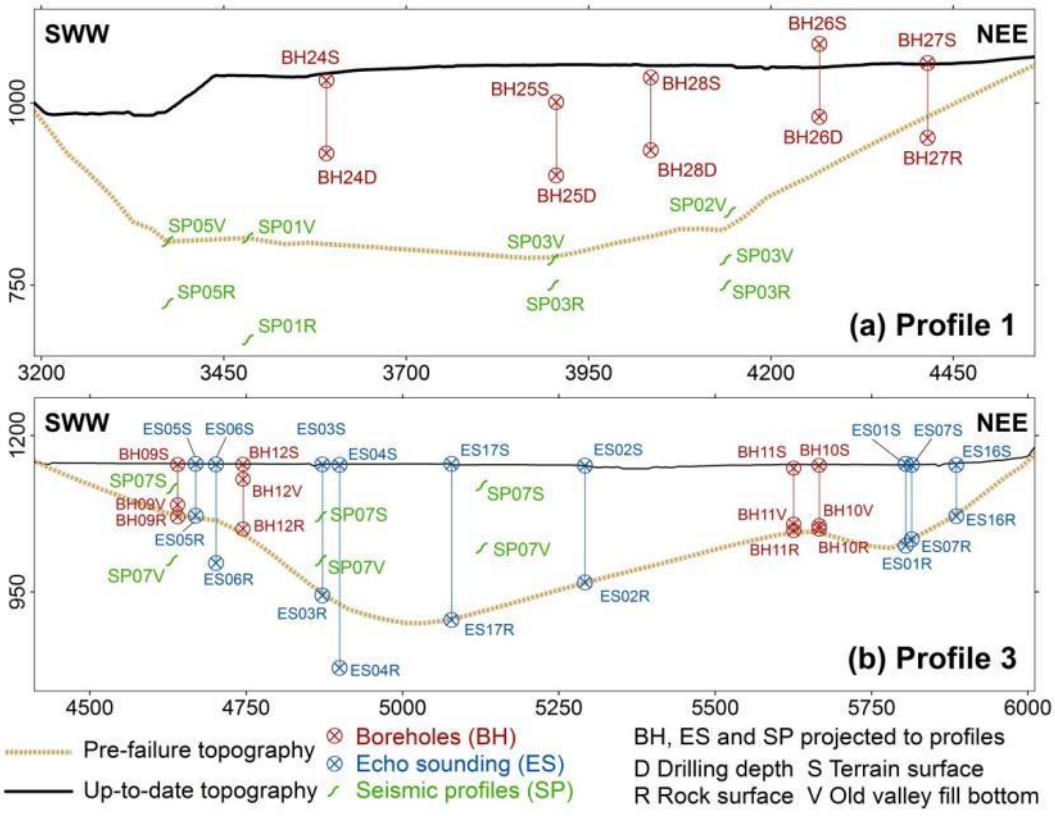

Figure 4: Profiles through the valley bottom in the Köfels Rock Slide area (see Figs. 2 and 3). (a) Profile 1 in the north of the Köfels site, basin of Umhausen. (b) Profile 3 in the south of the Köfels site, basin of Längenfeld. Note that the point data and seismic profiles (see Fig. 3) are projected to the profile planes and therefore do not necessarily correspond to the topographic surfaces shown.

https://doi.org/10.5194/nhess-2020-234
Preprint. Discussion started: 9 September 2020

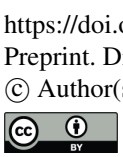

Natural Hazards and Earth System Sciences
Discussions

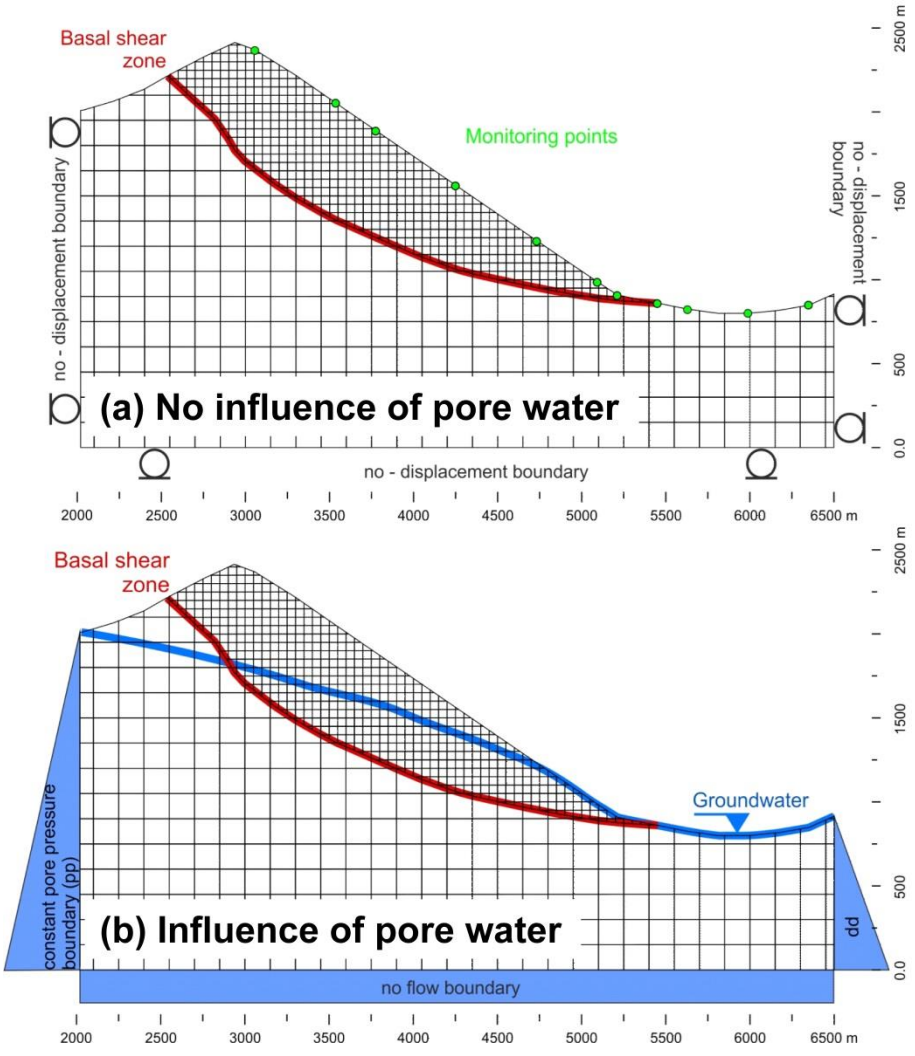

635 Figure 5: Model geometry with boundary conditions, joint sets for the failure rock mass and the underlying rock mass. (a) shows the monitoring points where deformations are recorded. (b) shows the groundwater table applied to the modelling scenario (B) assuming the typical trend of groundwater flow in slopes.

https://doi.org/10.5194/nhess-2020-234
Preprint. Discussion started: 9 September 2020

Natural Hazards and Earth System Sciences
Discussions

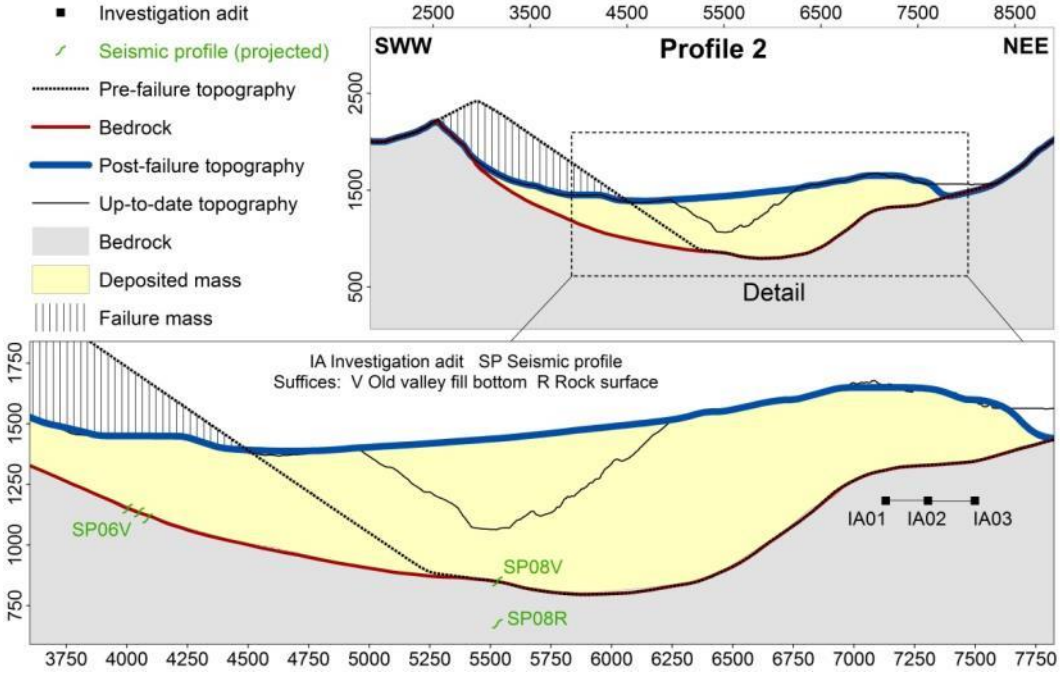

640 Figure 6: Profile 2 (see Figs. 2 and 3) through the Köfels site with the three reconstructed stages and the up-to-date topography.

https://doi.org/10.5194/nhess-2020-234
Preprint. Discussion started: 9 September 2020

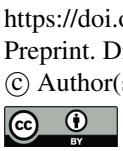

Natural Hazards and Earth System Sciences
Discussions

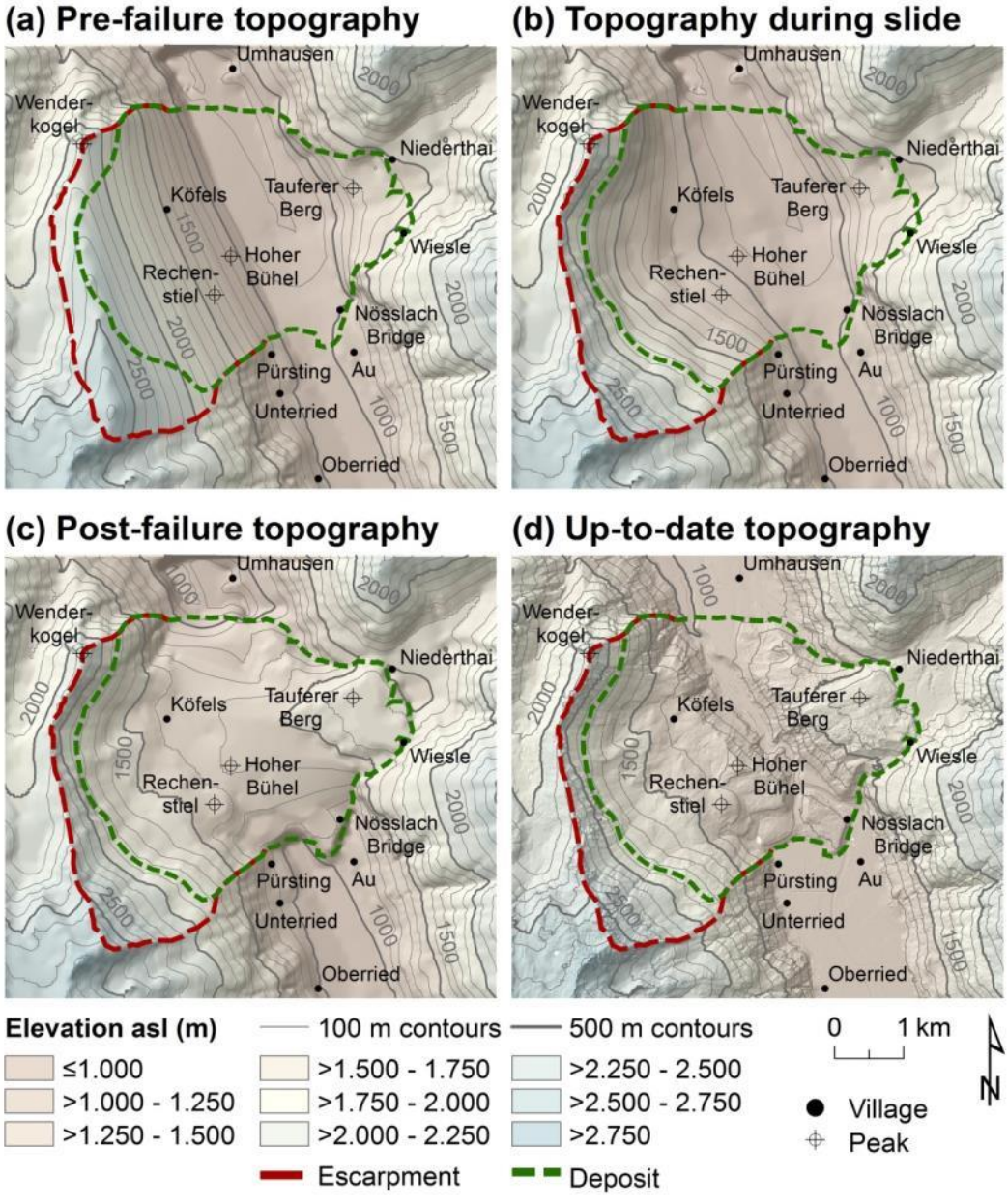

Figure 7: DEM of the three reconstructed stages and the up-to-date topography. (a) pre-failure, (b) bedrock, (c) post-failure, (d) up-to-date. The spatial resolution of the DEMs is 30 m in (a)–(c) and 1 m in (d).

https://doi.org/10.5194/nhess-2020-234
Preprint. Discussion started: 9 September 2020

Natural Hazards and Earth System Sciences
Discussions

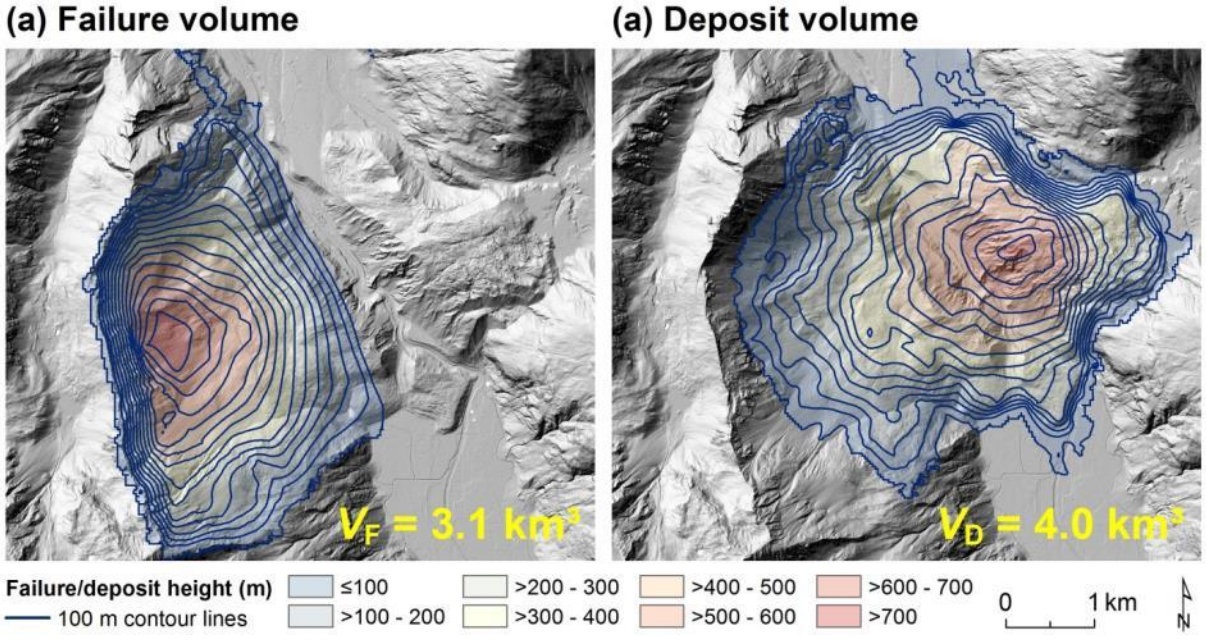

Figure 8: (a) Failure and (b) deposition heights and volumes of the Köfels Rock Slide mass computed in ArcGIS. The contour lines indicate the height difference between the (a) pre-failure and (b) post-failure topography and the topography of the sliding surface.

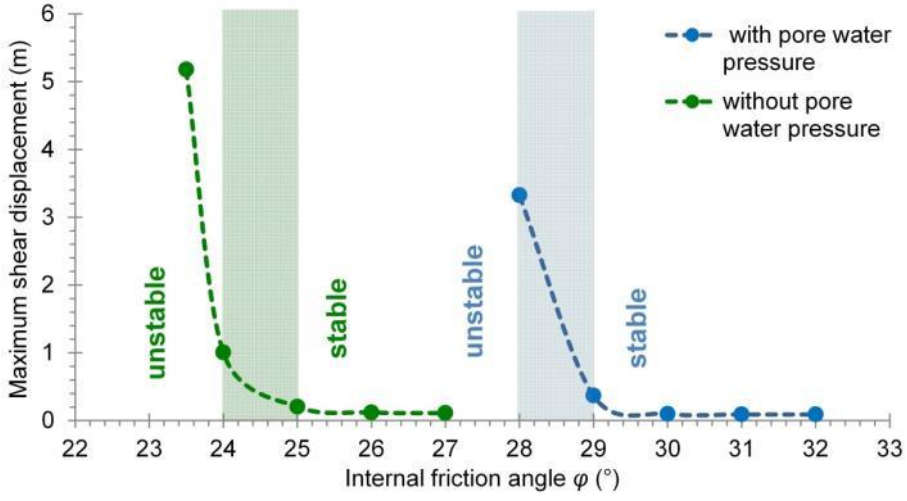

Figure 9: Results of the back-calculations with and without pore water pressure: the transition between failure and stable conditions without pore water pressure (scenario A) is found at φcrit = 24–25°. Applying pore water pressure to the model (scenario B) increases this transition zone to φcrit = 28–29°.

https://doi.org/10.5194/nhess-2020-234
Preprint. Discussion started: 9 September 2020

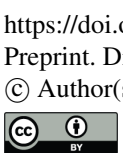

Natural Hazards and Earth System Sciences
Discussions

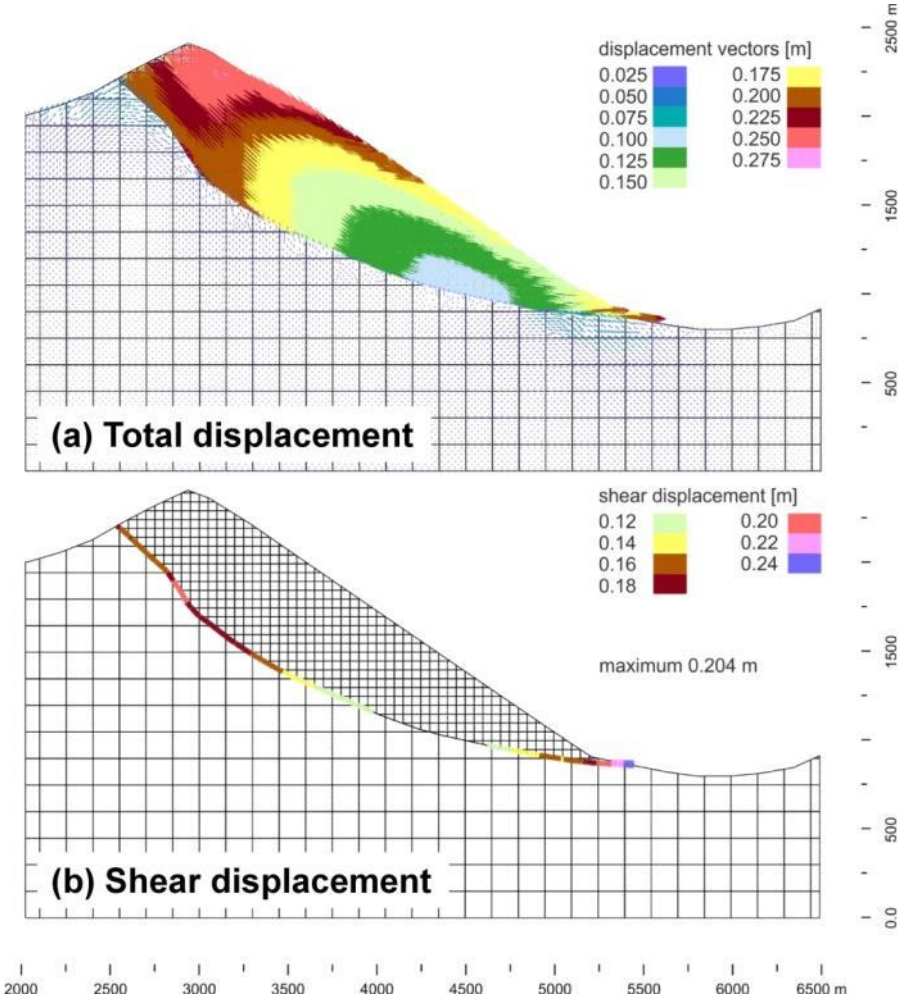

Figure 10: Spatial distribution of (a) total displacement and (b) shear displacement for φ = 25° for the modelling scenario (A) without pore water pressure.

https://doi.org/10.5194/nhess-2020-234
Preprint. Discussion started: 9 September 2020

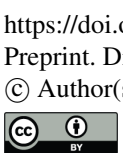

Natural Hazards and Earth System Sciences
Discussions

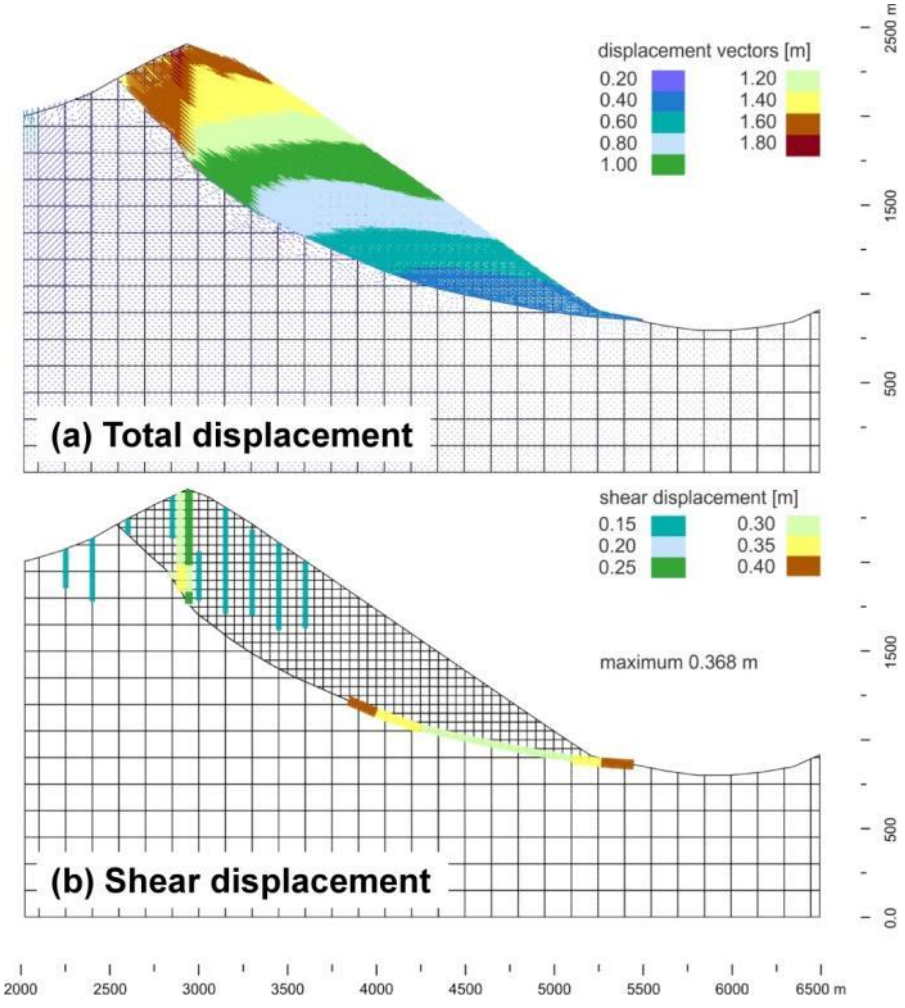

Figure 11: Spatial distribution of (a) total displacement and (b) shear displacement for φ = 29° for the modelling scenario (B) with pore water pressure.

https://doi.org/10.5194/nhess-2020-234
Preprint. Discussion started: 9 September 2020

Natural Hazards and Earth System Sciences Discussions

665 **Tables**

Table 1. Intact rock and discontinuity properties for the discontinuum distinct-element analysis, categorized into rock slide mass, underlying rock mass and basal shear zone (a_{zero}, a_{res} and j_{perm} are only relevant for modelling scenario (B) considering groundwater flow, all other parameters are the same for the modelling scenarios (A) and (B)).

Material property	Rock slide mass	Underlying rock mass	Basal shear zone
Density ρ (kg/m³)	2600	2600	–
Bulk modulus K (GPa)	22	22	–
Shear modulus G (GPa)	17	17	–
Discontinuity normal stiffness j_{kn} (GPa/m)	100	100	100
Discontinuity shear stiffness j_{ks} (GPa/m)	100	100	100
Discontinuity cohesion c (Pa)	0	0	0
Discontinuity friction angle φ (°)	30	30	Varied 20–27 and 26–32
Aperture for zero normal stress a_{zero} (m)	0.00018	0.00026	0.00026
Residual aperture at shear stress a_{res} (m)	0.00018	0.00026	0.00026
Discontinuity permeability constant j_{perm} (1/Pa s)	83.3	83.3	83.3

670